

An Analysis of the Stretching Mechanism of a Liquid Bridge in Typical Problems of Dip-Pen Nanolithography By Using Computational Fluid Dynamics

Cheng Zhang^{1,*} and Mingge Wu¹

Abstract: A computational study of the stretching mechanism of a liquid bridge and the effect of the liquid properties on the DPN (dip-pen nanolithography) process is presented. The results show that the viscosity and contact angle can have an appreciable influence on these processes. The greater the viscosity, the harder the liquid bridge is to break, which allows more molecular transfer during the DPN spotting process. Besides, when the contact angle between the liquid and substrate is less than 60 degrees, the time required to stretch the bridge and break it grows with the contact angle. During the stretching process, the pressure in the midsection (along the vertical direction) of the liquid bridge is relatively unstable, with frequent changes in its value. Furthermore, this pressure increases sharply when the liquid bridge breaks.

Keywords: DPN, liquid bridge, CFD, nanotechnology.

1 Introduction

With the continuous development of nanotechnology and micro-nano devices, it is very important to fabricate nanostructures or patterns with specific functions on the surface of the substrate [Tokura, Harvey, Chen et al. (2018); Khan, Han, Khan et al. (2018); Wen, Guo and Liu (2017); Ambrosi and Pumera (2016)]. DPN (dip-pen nanolithography) has become the mainstream and important nanostructure fabrication technology for the past ten years [Ma, Jiang, Xie et al. (2018)]. The principle of DPN is shown in Fig. 1 [Basnar and Willner (2009)]: The atomic force (AFM) probe is used to extract the molecules and make the molecules evenly distributed on the surface of the AFM probe. When the tip of the probe is close to the surface of the substrate, a liquid bridge is formed between the probe and substrate, and then the molecules are transferred from the tip of the atomic force tip to the substrate by capillary forces [Arrabito, Reisewitz, Dehmelt et al. (2013)]. The atomic force microscope precisely controls the positioning and two-dimensional movement of the tip on the substrate to form a nanoscale pattern [Ginger, Zhang and Mirkin (2004)], and the minimum pattern can be made up to 10~15 nm [Zhong, Sun and He (2014)].

¹ College of Mechanical and Electrical Engineering, Wenzhou University, Wenzhou, 325035, China.

* Corresponding Author: Cheng Zhang. Email: zhangcheng0630@126.com.

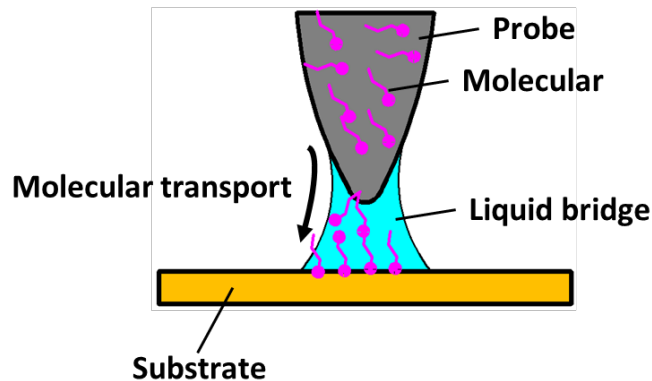


Figure 1: Schematic diagram of the dip-pen nanolithography processing

Due to the simple and efficient advantages of DPN in direct writing nanostructures, the enthusiasm of researchers has been aroused, and the mechanism and influencing factors of DPN transfer process have been analyzed. For examples, Wu et al. [Wu and Fang (2011)] have studied the deposition of ink molecules on rough substrates in dip-pen nanolithography by using molecular dynamics (MD) simulations. Kim et al. [Kim, Saha, Saha et al. (2010)] studied the effect of meniscus structure in DPN by using an atomistic molecular dynamics simulation. Heo et al. [Heo, Yang, Kim et al. (2009)] found that increasing the molecular-substrate binding energy can increase the rate of molecular deposition and make the monolayer order. However, the current experiments and simulations focus on the molecular transfer process and lack the influence of the corresponding liquid bridge on the direct writing process. Therefore, this paper is to study the process of liquid bridge stretching and fracture during DPN process, and analyzes the effect of liquid viscosity and contact angle on DPN transfer base on computational fluid dynamics.

2 Calculation method and model

2.1 Calculation model

We simplified the initial phase of the DPN fluid into a geometric model as shown in Fig. 2(a), with the solid upper and lower plane (the upper plane correspond to the probe in Fig. 1 and the lower plane to the substrate), the middle part is liquid (corresponding to the liquid bridge in the DPN), in which the substrate is fixed and the probe moves upwards at a constant speed. Also, it is assumed that the liquid is completely adhered to the substrate and the probe. Moreover, the process of solid-liquid phase change is not considered. In addition, we set the length of the upper and lower planes in the geometric model to be $L=20\ \mu\text{m}$, the distance $D=8\ \mu\text{m}$, and the contact angle $\alpha=45^\circ$. Fig. 2(b) is the Grid of fluid computing domain, the type of grid is square. And we encrypted the mesh of the liquid bridge part, which helps the result to be more accurate. The middle part of Fig. 2(b) is the grid refinement study is added in this study, and the grid refinement part is the liquid bridge.

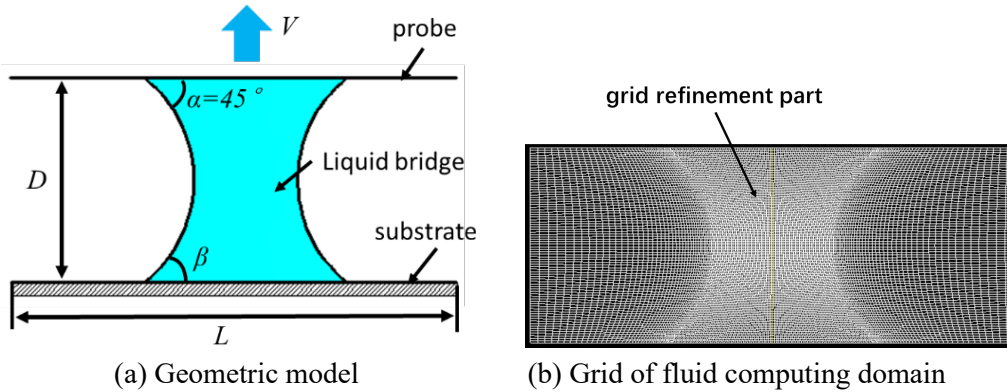


Figure 2: Geometric model and grid of the initial stage of the stretched flow field

2.2 Boundary conditions

Base on the geometric model and grid of the initial stage of the stretched flow field, we import the grid file into Ansys Fluent 14.5 for boundary condition settings. The VOF model was selected as the multiphase flow model, air was defined as the basic phase of the model, and the liquid containing the solid molecules was defined as the second phase, the liquid density was set to 1000 kg/m^3 , and the viscosity was $0.005 \text{ Kg/m}\cdot\text{s}$. At the same time, consider the surface tension of the liquid and air, and set the surface tension coefficient to 1 N/m . In addition, we also consider the influence of the contact angle, set the contact angle β to 45° , set the left boundary as the pressure inlet, the right boundary as the symmetry plane, the pressure value as atmospheric pressure, and set the gravity to 9.8 m/s^2 , we set the upper boundary to the dynamic mesh, and the mesh movement method is layering. And UDF programming is used to make the upper boundary achieve a uniform speed of 0.2 m/s . In addition, the non-steady state calculation was used, the time step was set to $0.05 \mu\text{s}$, and the liquid phase change of the fluid stretching process during the simulation was recorded in real time using the recording function provided by Ansys Fluent 14.5.

2.3 Calculation method

In this study, the study object is a two-phase fluid that includes both liquid and gas (air). The conservation equation is as follows:

$$\frac{\partial(\rho u)}{\partial t} + \nabla(\rho u \times u) = -\nabla P + \nabla(\mu \nabla \times u) + F_g + F_s \quad (1)$$

$$\nabla(\rho u) = 0 \quad (2)$$

where: ρ is density; t is time; u is velocity vector; P is pressure; μ is dynamic viscosity; F_g and F_s is gravity and surface tension, respectively.

The expression of the surface tension F_s is as follows:

$$F_s = \sigma \kappa n \quad (3)$$

where σ represents the surface tension coefficient; κ represents the free surface curvature; n represents the unit normal vector of the free surface:

$$\mathbf{n} = \frac{\nabla F}{|\nabla F|} \quad (4)$$

$$\kappa = -(\nabla \cdot \mathbf{n}) \quad (5)$$

where: ∇ denotes a gradient operator perpendicular to the direction of the free surface.

The VOF method is used to record the volume fraction of each calculation unit. Scardovelli and Zaleski have showed that the VOF method can accurately handle free surface problems [Scardovelli and Zaleski (1999)]. The volume fraction of liquid in the VOF process is represented by F , which is defined as: $F=1$ means located in the liquid phase; $0 < F < 1$ means on the free surface; $F=0$ means in the gas phase.

Equation of motion:

$$\frac{\partial F}{\partial t} + (\mathbf{u} \times \nabla) F = 0 \quad (6)$$

The free surface is constructed by a second-order piecewise linear interface structure (PLIC). The density ρ and dynamic viscosity μ of the free surface fluid are calculated by:

$$\rho = F\rho_l + (1 - F)\rho_a \quad (7)$$

$$\mu = F\mu_l + (1 - F)\mu_a \quad (8)$$

The subscripts “ l ” and “ a ” indicate the liquid bridge and air, respectively.

This study uses the Carreau model to describe the shear thinning effect of the ink, expressed as follows:

$$\mu_l = \mu_{0,l} [1 + (\lambda \varepsilon)^2]^{\frac{n-1}{2}} \quad (9)$$

where: $\mu_{0,l}$ represents the viscosity of the ink when the shear rate is 0; λ represents the duration; n represents the Carreau index;

The shear rate ε is defined as:

$$\varepsilon = \frac{\partial u_x}{\partial y} + \frac{\partial u_y}{\partial x} \quad (10)$$

3 Results and discussion

3.1 The stretching and breaking process of the liquid bridge during DPN

Based on the above calculation methods, model and boundary conditions, the liquid phase diagram of the liquid bridge stretching and fracture process was studied, and the result shown in Fig. 3. As we can see, when the probe moves upward at a uniform speed, the liquid bridge is stretched and relative thinned at the middle section of the liquid bridge. Moreover, as the stretching continues, the fluid begins to break. Because of the action of surface tension, the fracture liquid will shrink into a semicircular droplet on the upper and lower planes after the liquid bridge been broken. Further, Fig. 3 is calculated under the contact angle β of 45° , so the contact angle of the liquid on the upper and lower surfaces is the same, which means the influence of the liquid on the upper and lower sides is the same, so the droplets are formed on the upper and lower surfaces in a similar size. In addition, as can be seen from Fig. 3, the liquid concentration of the liquid bridge and air interface in the stretching process is smaller than the middle position of the liquid bridge, indicating that the gas may have an influence on the liquid bridge stretching in the DPN, so we analyzed the effect of gas on the liquid bridge below.

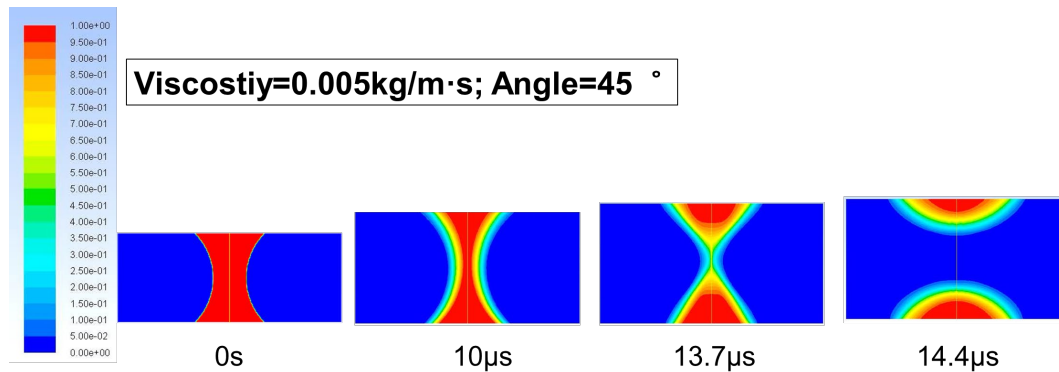


Figure 3: Liquid phase diagram of the stretching and breaking process of the liquid bridge during DPN

3.2 The total pressure distribution of the liquid bridge during the DPN process

Based on the above calculation method, the total pressure distribution cloud diagram of the tension and fracture process of the liquid bridge in the DPN process is obtained by simulation. It can be seen from Figs. 5(a) and 5(b) that the inside of the liquid bridge during the drawing process is a negative pressure, and the internal pressure value is lower than the external atmospheric pressure. As can be seen from Figs. 5(c) and 5(d), the internal pressure of the liquid becomes a positive pressure at the time of the breaking, and the internal pressure value is higher than the external atmospheric pressure, so that the liquid bridge pressure changes greatly during the stretching. In addition, as can be seen from Fig. 5(d), the internal pressure of the liquid bridge tends to decrease after breaking, but it is still greater than the atmospheric pressure. In summary, the pressure in the liquid bridge changes greatly during the DPN stretching process. Therefore, we studied the changes of the internal total pressure in the liquid bridge in detail below.

In order to more accurately analyze the internal pressure changes of the liquid during the stretching process. We monitored and sampled the pressure on the central axis (vertical direction) of the liquid bridge stretch and fracture moments with a liquid density of 1000 kg/m³, a viscosity of 0.005 Kg/m·s and a contact angle β of 45°. Fig. 6(a) is the pressure distribution of the axis during the stretching process (stretching time is 10 µs). It can be seen from the figure that the pressure in the middle position of the liquid bridge during the stretching process is relatively unstable, and the pressure jump is frequent. In addition, the pressure near the probe is large. Fig. 6(b) shows the pressure distribution at the center of the fracture time (stretching time is 3 µs). As can be seen from the figure, total pressure of the intermediate of the liquid bridge increases sharply at the time of the break moment.

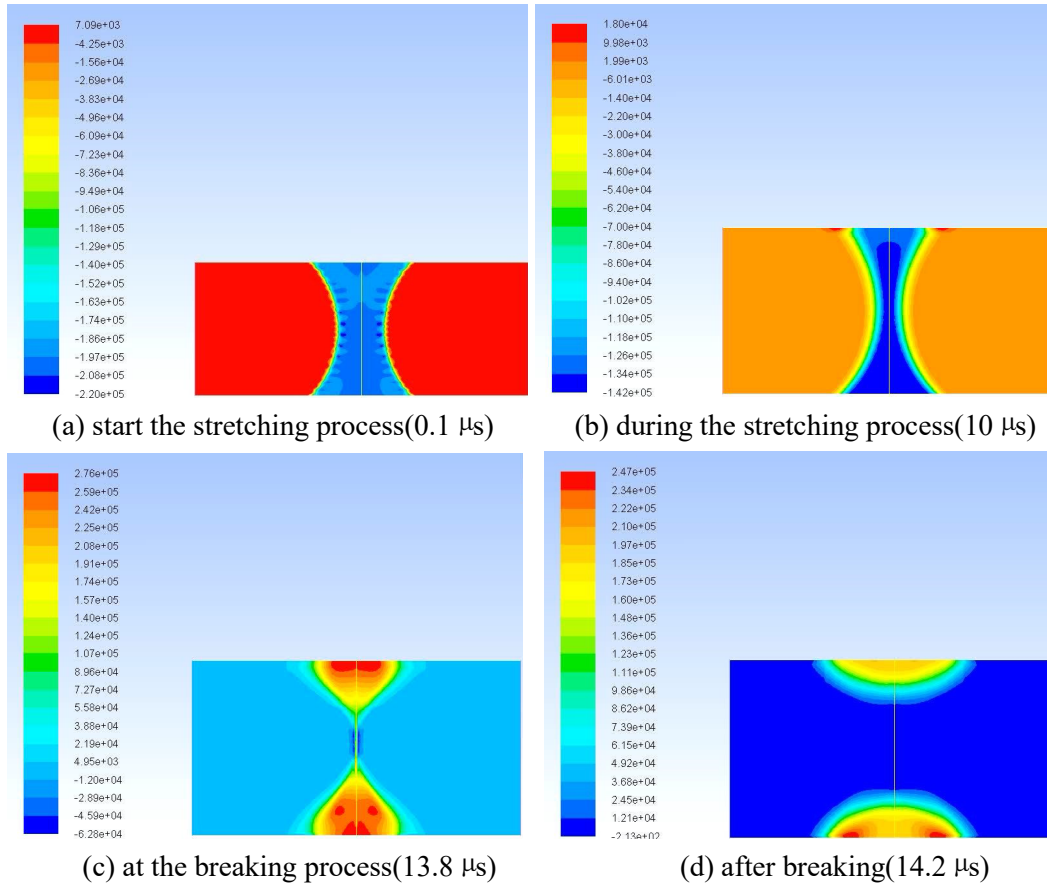


Figure 5: Total pressure distribution of the liquid bridge during the DPN process

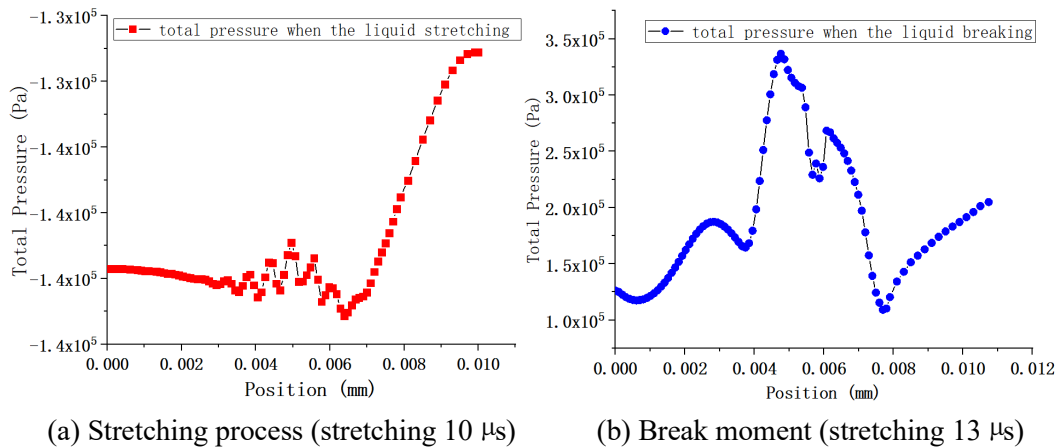
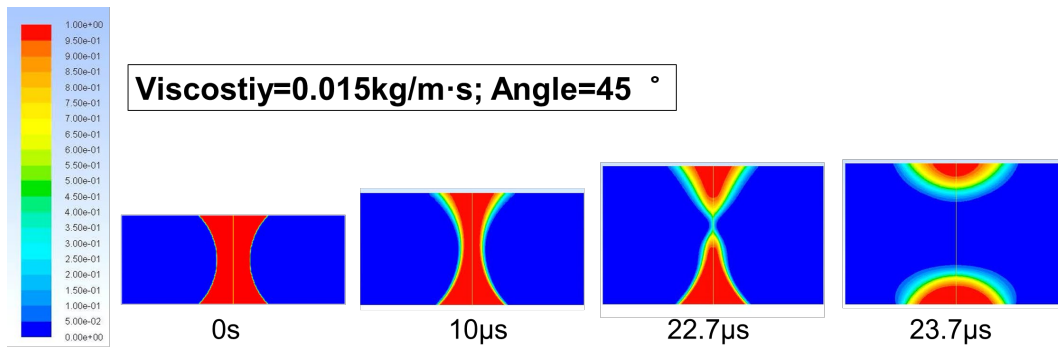


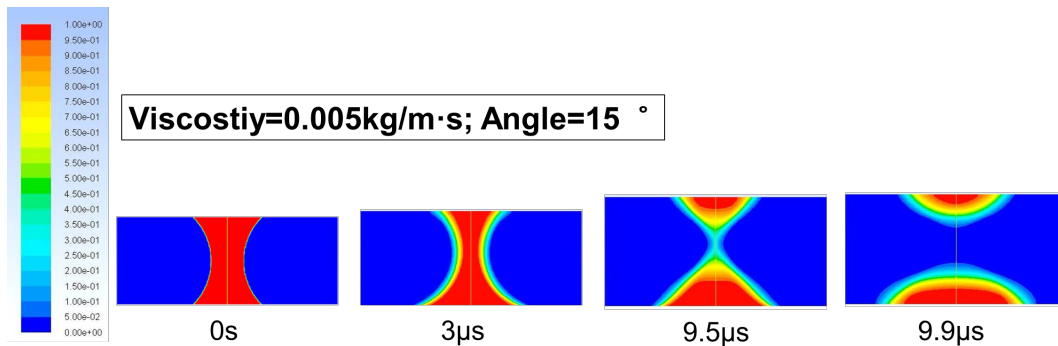
Figure 6: Total pressure distribution on the central axis (vertical direction) of the liquid bridge

3.3 Effect of viscosity and contact angle on the DPN process

The viscosity and contact angle β is the important influencing factors on the DPN process, so we calculated the stretching of liquids under different liquid viscosities and different contact angles. Fig. 7(a) is calculated under the condition of viscosity is 0.01 Kg/m·s and contact angle β is 45° . Fig. 7(b) is calculated under the condition of viscosity is 0.005 Kg/m·s and contact angle β is 15° . Comparing Fig. 7(a) with Fig. 3(a) we can get that the greater the viscosity of liquid, the harder the liquid is to break, and more time it takes from stretching to breaking, which means the longer it could be stretched. However, a liquid bridge having a large viscosity forms a small droplet on the surface of the substrate. Comparing Fig. 7(b) with Fig. 3(a) we can get that the smaller the contact angle, the more easily liquid bridge breaks, and the less time it takes from stretching to breaking. However, the liquid bridge with a small contact angle has a large droplet formed on the surface of the substrate. In order to analyze the influencing factors of viscosity and contact angle in more detail, we performed multiple sets of simulation calculations below.



(a) Viscosity=0.015 kg/m·s; Angle= 45°



(b) Viscosity=0.005 kg/m·s; Angle= 15°

Figure 7: Liquid phase diagram of the stretching and breaking process of the liquid bridge during DPN

In order to study the effects of viscosity and contact angle on fluid stretching and fracture process in detail, several sets of simulation studies were carried out, and the simulation results were statistically analyzed. The specific calculation parameters are shown in Tab. 1 and Tab. 2.

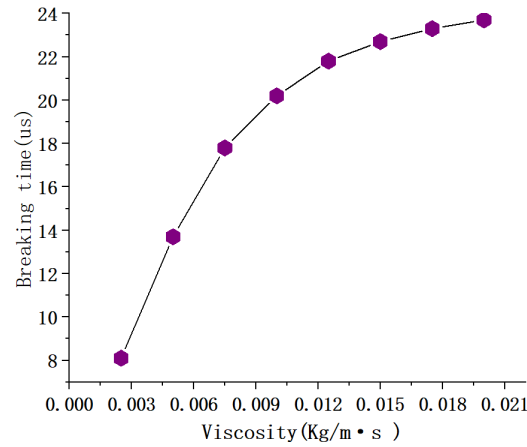
Table 1: Calculation parameters of different liquid viscosity

Parameter	Viscosity η (Kg/m·s)	Density ρ (kg/m ³)	Velocity V (m/s)	Contact α (°)
Value	0.025, 0.005, 0.075, 0.01, 0.0125, 0.015 0.0175, 0.02	1000	0.2	45

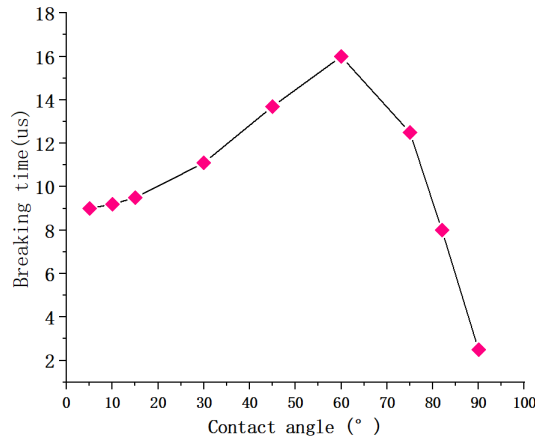
Table 2: Calculation parameters of different contact angles

Parameter	Viscosity η (Kg/m·s)	Density ρ (kg/m ³)	Velocity V (m/s)	Contact α (°)
Value	0.005	1000	0.2	5, 10, 15, 30, 45, 60, 75, 82, 90

Based on the above calculation parameters, we got the effects of viscosity and contact angle on the DPN process. As shown in Fig. 8(a), the relationship between viscosity and fracture time shows that it takes longer time for the high-viscosity fluid to be broken than the low-viscosity fluid. Since the elongation l is obtained by multiplying the stretching speed V by the breaking time t , that is, $l=V \times t$ ($V=0.2$ m/s), the high-viscosity liquid bridge is pulled longer when it is stretched to break. Moreover, the tensile deformation of fluids at different contact angles is also analyzed. Fig. 8(b) shows the relationship between viscosity and fracture time. As can be seen from the figure, when the contact angles are less than 60 degree, the larger contact angle the longer the time required to stretch it to break, and also the longer the fluid is stretched. But when the contact angles are larger than 60 degree, the larger contact angle the less time required to stretch it to break, and the shorter the fluid is stretched.



(a) Relationship between viscosity and fracture time



(b) Relationship between contact angle and fracture time

Figure 8: Effects of viscosity and contact angle on the DPN process

5 Conclusion

The stretching mechanism of liquid bridge and the effect of liquid properties on DPN process based on computational fluid dynamics (CFD) was studied. The result shows, the viscosity and contact angle have certain effects on the liquid bridge stretching and fracture process. The greater the viscosity, the harder the liquid bridge is to break, which allows more molecular transfer during the DPN spotting process. Besides, when the contact angles are less than 60 degrees, the larger contact angle the longer the time required to stretch it to break, and the longer the fluid is stretched. When the contact angles are larger than 60 degrees, the larger contact angle the less time required to stretch it to break, and the shorter the fluid is stretched. During the stretching process, the pressure in the middle position (vertical direction) of the liquid bridge is relatively

unstable, and the pressure changes frequently. Besides, the intermediate pressure of the liquid bridge increases sharply in the breaking moment, and the liquid concentration of the liquid bridge and air interface in the stretching process is smaller than the middle position of the liquid bridge. Moreover, the intermediate pressure of the liquid bridge increases sharply.

Acknowledgement: This paper is funded by the basic scientific research project of Wenzhou, China (No. G20190014). And supported by Key Laboratory of Air-driven Equipment Technology of Zhejiang.

References

- Ambrosi, A.; Pumera, M.** (2016): Templated electrochemical fabrication of hollow molybdenum sulfide microstructures and nanostructures with catalytic properties for hydrogen production. *ACS Catalysis*, vol. 6, no. 6, pp. 3985-3993.
- Arrabito, G.; Reisewitz, S.; Dehmelt, L.; Bastiaens, P. I.; Pignataro, B. et al.** (2013): Biochips for cell biology by combined dip-pen nanolithography and DNA-directed protein immobilization. *Small*, vol. 9, no. 24, pp. 4243-4249.
- Basnar, B.; Willner, I.** (2009): Dip-pen-nanolithographic patterning of metallic, semiconductor, and metal oxide nanostructures on surfaces. *Small*, vol. 5, no. 1, pp. 28-44.
- Ginger, D. S.; Zhang, H.; Mirkin, C. A.** (2004): The evolution of dip-pen nanolithography. *Angewandte Chemie International Edition*, vol. 43, no. 1, pp. 30-45.
- Heo, D. M.; Yang, M.; Kim, H.; Saha, L. C.; Jang, J.** (2009): Tip dependence of the self-assembly in dip-pen nanolithography. *Journal of Physical Chemistry C*, vol. 113, no. 31, pp. 13813-13818.
- Khan, M. E.; Han, T. H.; Khan, M. M.; Karim, M. R.; Cho, M. H.** (2018): Environmentally sustainable fabrication of Ag@ g-C₃N₄ nanostructures and their multifunctional efficacy as antibacterial agents and photocatalysts. *ACS Applied Nano Materials*, vol. 1, no. 6, pp. 2912-2922.
- Kim, H.; Saha, L. C.; Saha, J. K.; Jang, J.** (2010): Molecular simulation of the water meniscus in dip-pen nanolithography. *Scanning: Journal of Scanning Microscopies*, vol. 32, no. 1, pp. 2-8.
- Ma, H.; Jiang, Z.; Xie, X.; Huang, L.; Huang, W.** (2018): Multiplexed biomolecular arrays generated via parallel Dip-Pen nanolithography. *ACS Applied Materials & Interfaces*, vol. 10, no. 30, pp. 25121-25126.
- Scardovelli, R.; Zaleski, S.** (1999): Direct numerical simulation of free-surface and interfacial flow. *Annual Review of Fluid Mechanics*, vol. 31, no. 1, pp. 567-603.
- Tokura, Y.; Harvey, S.; Chen, C.; Wu, Y.; Ng, D. Y. et al.** (2018): Fabrication of defined polydopamine nanostructures by DNA origami-templated polymerization. *Angewandte Chemie International Edition*, vol. 57, no. 6, pp. 1587-1591.
- Wu, C. D.; Fang, T. H.** (2011): Simulation of deposition of ink molecules on rough substrates in dip-pen nanolithography. *Modelling and Simulation in Materials Science and Engineering*, vol. 19, no. 6, pp. 065008.

Wen, G.; Guo, Z.; Liu, W. (2017): Biomimetic polymeric superhydrophobic surfaces and nanostructures: from fabrication to applications. *Nanoscale*, vol. 9, no. 10, pp. 3338-3366.

Zhong, J.; Sun, G.; He, D. (2014): Classic, liquid, and matrix-assisted dip-pen nanolithography for materials research. *Nanoscale*, vol. 6, no. 21, pp. 12217-12228.